IEEE Access
Multidisciplinary ⋮ Rapid Review ⋮ Open Access Journal

Received 7 December 2023, accepted 21 December 2023, date of publication 25 December 2023, date of current version 4 January 2024.

Digital Object Identifier 10.1109/ACCESS.2023.3346894

RESEARCH ARTICLE

Improved Water Strider Algorithm With Convolutional Autoencoder for Lung and Colon Cancer Detection on Histopathological Images

HAMED ALQAHTANI[1], EATEDAL ALABDULKREEM[2], FAIZ ABDULLAH ALOTAIBI[3], MRIM M. ALNFIAI[4], CHINU SINGLA[5], AND AHMED S. SALAMA[6]

[1]Department of Information Systems, Center of Artificial Intelligence, College of Computer Science, King Khalid University, Abha 62529, Saudi Arabia
[2]Department of Information Systems, College of Computer and Information Sciences, Princess Nourah bint Abdulrahman University, P.O. Box 84428, Riyadh 11671, Saudi Arabia
[3]Department of Information Science, College of Arts, King Saud University, P.O. Box 28095, Riyadh 11437, Saudi Arabia
[4]Department of Information Technology, College of Computers and Information Technology, Taif University, Taif 21944, Saudi Arabia
[5]Department of Computer Science, University of the People, Pasadena, CA 91101, USA
[6]Department of Electrical Engineering, Faculty of Engineering and Technology, Future University in Egypt, New Cairo 11845, Egypt

Corresponding author: Mrim M. Alnfiai (m.alnofiee@tu.edu.sa)

This work was supported in part by the Deanship of Scientific Research at King Khalid University through Large Group Research Project under Grant RGP2/153/44; in part by the Princess Nourah bint Abdulrahman University Researchers Supporting Project, Princess Nourah bint Abdulrahman University, Riyadh, Saudi Arabia, under Grant PNURSP2023R161; in part by the Research Supporting Project, King Saud University, Riyadh, under Grant RSPD2024R838; and in part by the Future University in Egypt (FUE).

ABSTRACT Lung and colon cancers are deadly diseases that can develop concurrently in organs and undesirably affect human life in some special cases. The detection of these cancers from histopathological images poses a complex challenge in medical diagnostics. Advanced image processing techniques, including deep learning algorithms, offer a solution by analyzing intricate patterns and structures in histopathological slides. The integration of artificial intelligence in histopathological analysis not only improves the proficiency of cancer detection but also holds the potential to increase prognostic assessments, eventually contributing to effective treatment strategies for patients with lung and colon cancers. This manuscript presents an Improved Water Strider Algorithm with Convolutional Autoencoder for Lung and Colon Cancer Detection (IWSACAE-LCCD) on HIs. The major aim of the IWSACAE-LCCD technique aims to detect lung and colon cancer. For noise removal process, median filtering (MF) approach can be used. Besides, deep convolutional neural network based MobileNetv2 model can be applied as a feature extractor with IWSA based hyperparameter optimizer. Finally, convolutional autoencoder (CAE) model can be applied to detect the presence of lung and colon cancer. To enhance the detection results of the IWSACAE-LCCD technique, a series of simulations were performed. The obtained results highlighted that the IWSACAE-LCCD technique outperforms other approaches in terms of different measures.

INDEX TERMS Medical image analysis, histopathological images, cancer detection, machine learning, deep learning.

I. INTRODUCTION

Lung and colorectal (colon and rectum) cancers are the most common varieties around the world following breast tumors, with cancer rates of 11.4% and 10% correspondingly in 2020 [1]. Even though lesser, there is a possibility of synchronous taking place among lung and colon cancers (LCC). Furthermore, LCC outperforms the top 2 mortality rates of 18% and 9.4% correspondingly between each cancer [2]. Thus, highly accurate detection of these cancer sub-types is required to

The associate editor coordinating the review of this manuscript and approving it for publication was Wai-Keung Fung.

analyse the therapeutic method in the early phases of cancer [3]. The non-invasive techniques to diagnose include computed tomography (CT) images and radiography for lung cancer and CT colonoscopy, as well as adaptable sigmoidoscopy for colon cancer [4], [5]. But, dependable sub-categories of these cancers might be impossible by utilizing non-invasive procedures continually, and slightly invasive methods namely histopathology can be needed for accurately detecting cancers and enhancing treatment quality. For pathologists, the manual grading of histopathological images (HI) is found to be difficult and time-consuming [6]. Also, an exact grading of the LCC sub-classes needs skilled pathologists, and manual grading is subject to error. Therefore, automatic image processing approaches for LCC images have been affirmed to decrease the problem for pathologists [7], [8].

In recent years, a wide-ranging development of technological prospects in biomedical applications for treatment and diagnosis methods of cancer kinds [9]. The decision-making method of medical experts could take an extended period in the diagnostic procedure of cancer patients. In this scenario, artificial intelligence (AI) technology gives the chance to make decisions by analyzing data more rapidly [10], [11]. In this case, the data containing the HI of LCCs are analyzed. Cancer varieties are identified by employing a deep learning (DL) technique that can be a sub-group of AI, with optimization algorithms. Additionally, diagnosing cancer cases proceeds for a long period and depends on various thoughts of physicians, particularly in the earlier phases [12]. A specific domain of the medical field can address these challenges. AI approaches are employed in the medical sector namely earlier diagnosis of biomedical images, disease prediction, medical emergencies, and so on [13], [14], [15]. In addition, DL approaches extracted secret features and features in medical images, which could not be realised with the naked eye for timely identifying the cancers as well as differentiating among their phases.

This manuscript presents an Improved Water Strider Algorithm with Convolutional Autoencoder for Lung and Colon Cancer Detection (IWSACAE-LCCD) on HIs. The presented IWSACAE-LCCD technique aims to recognize and classify lung as well as colon cancers. In this developed IWSACAE-LCCD method, the noise removal process is executed by the median filtering (MF) approach. In addition, the deep convolutional neural network (DCNN) based MobileNetv2 model can be applied for deriving features and IWSA is employed for the hyperparameter tuning process. For cancer detection, the convolutional autoencoder (CAE) model can be used which identifies the occurrence of lung as well as colon cancer. To enhance the detection results of the IWSACAE-LCCD technique, a series of simulations were performed. Shortly, the key contributions can be given below.

- A new IWSACAE-LCCD algorithm comprising MF-based pre-processing, MobileNetv2 feature extractor, IWSA-based hyperparameter tuning, and CAE classifier could be developed for LCC detection. To better of our knowledge, the IWSACAE-LCCD approach is not presented in the literature.
- Develop a MobileNetv2 model for feature extraction from HIs that extracts relevant features crucial for accurate cancer detection. Besides, CAE excels at identifying the occurrence of both LCC in HIs, further enhancing the detection accuracy.
- Present IWSA for hyperparameter tuning optimizes the hyperparameters of the MobileNetv2, enhancing its performance and robustness in cancer detection tasks. The IWSA has been obtained by the combination of WSA with the oppositional-based learning (OBL) model.

II. LITERATURE REVIEW

Wahid et al. [16] presented a computer-assisted diagnosis (CAD) system employing the CNN approach for diagnosing LCCs. In this case, three pre-trained CNN methods are employed such as ResNet-18, GoogLeNet, ShuffleNet V2, and one simple adapted CNN algorithm. Karim and Bushra [17] focused on offering a CNN method, which is used for accurately identifying and classifying lung cancer varieties with higher accuracy that can be highly significant for treatment. Saif et al. [18] introduced a CNN to detect 3 categories of lung cancers (Squamous, Benign, and Adenocarcinoma) depending on HI. This technique contains major three subpaths. The major path performs for extracting the smaller features and generating feature maps at lower levels. The subpaths are accountable to change the higher and intermediate stages features map to fully connected (FC) layers for executing the classification method, and the VGG16 can be utilised for comparison.

In [19], the authors introduced a marine predator's algorithm with DL as an LCC classification (MPADL-LC3) approach. This approach targets to appropriately differentiate various kinds of LCCs. This algorithm utilizes contrast-limited adaptive histogram equalization (CLAHE)-based contrast development as a preprocessing stage. Moreover, MobileNet and MPA are utilized for deriving hyper-parameter optimizers and feature vector generation. Also, the deep belief network (DBN) is implemented for LCC classification. In the presented Hadiyoso et al. [21 developed a technique for automatically classifying LCCs depending on a DL method. The object of the image can be categorized, which is the HI of normal tissue, benign, and malignant cancers. CNN with VGG16 framework and CLAHE are utilized for validating classification on 25000 HI.

In [22], the authors recommended a CNN algorithm that represented quickness of analysis and higher accuracy with some count of parameters to diagnose colon adenocarcinoma. This method includes two paths that can be accountable for making 256 mapping features to improve the count of features at diverse levels for enhancing the sensitivity and accuracy of the classification. Besides, the VGG16 framework is designed and trained on a similar dataset. Kapoor et al. [23] proposed a unique technique to exploit HI for diagnosing LCCs. This suggested method employs CNNs for feature extraction and classification.

III. THE PROPOSED MODEL

In this manuscript, we have considered the development of the IWSACAE-LCCD technique for the identification and classification of LCC under HIs. The proposed IWSACAE-LCCD technique's purpose is to recognize and classify

LCC. The presented IWSACAE-LCCD technique comprises several subprocesses such as MF-based preprocessing, MobileNetv2 feature extractor, IWSA based hyperparameter tuning, and CAE-based cancer detection. Fig. 1 demonstrates the workflow of the IWSACAE-LCCD algorithm.

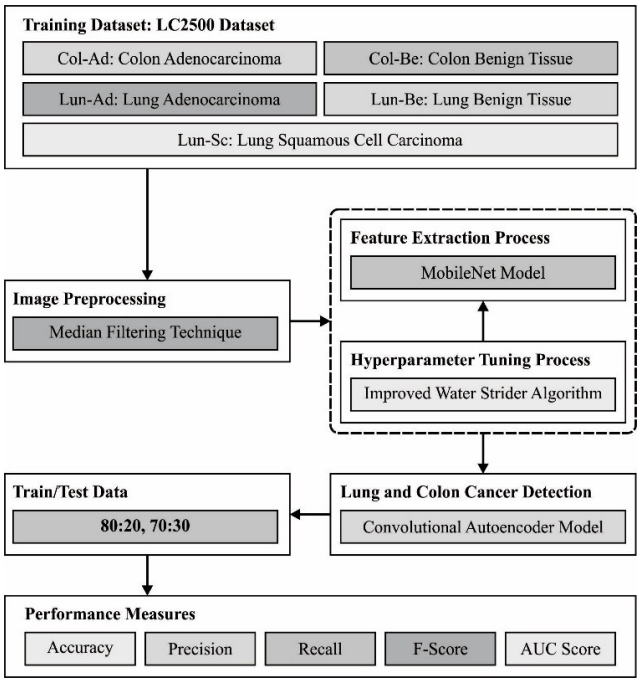

FIGURE 1. Workflow of the IWSACAE-LCCD approach.

A. IMAGE PREPROCESSING USING THE MF APPROACH

To eliminate the noise that arises in the input images, the MF approach can be applied. Particularly, it is effective in removing salt-and-pepper noise, which is a type of noise that arbitrarily changes certain pixels in the image to white or black. The procedure of using an MF to an image includes sliding a window of fixed size over the image, centring on all the pixels, and substituting the pixel values with the median value of the pixel within the window. Typically, the size of the window is an odd number to make sure that there is a centre pixel.

B. FEATURE EXTRACTION MODEL

To produce a collection of features in these preprocessed images, the MobileNetv2 architecture has been applied. MobileNetV2 is a CNN design for lightweight and effectual DL tasks, mostly suitable for embedded and mobile devices [24]. It is a development of the original MobileNet design, concentrating on enhancing efficacy but preserving competitive accuracy on distinct tasks such as object detection and image classification. MobileNetV2 accomplishes this effectiveness through a group of depth-wise separable convolutional, linear bottlenecks, and inverted residuals. The MobileNetV2 structure includes the ReLu component, a remaining layer can have a stride of 1 along the downsized layer has a stride of 2. The downsizing and remaining layers contain 3 sub-layers each.

- The 1×1 convolutional layer with *ReLu*6 is the initial layer.
- Depthwise Convolutional layer is the second layer
- The Depthwise layer includes a single convolution layer, which implements a trivial filtering model.
- Without non-linearity, the 1×1 Convolution layer is the third layer. Here, the *ReLu* module is utilized in the outcome.
- Rectified linear units (ReLu) and improvising the randomness of the network ensure the robustness utilized in low-precision situations.
- Every individual layer has a similar amount of output channels.
- The size of 3×3 convolutional filters is common for the overall models, and during the training phase, batch normalization and dropout layers are used.

C. HYPERPARAMETER TUNING MODEL

At this stage, the IWSA is designed to select the hyperparameters of the MobileNetv2 model. The birth stage is the initial phase of WSA [25]. Here, the male water striders (WSs) which are otherwise called keystones carry out mating to produce the eggs (population initialization). The mathematical expression of this process can be formulated by using Eq. (1):

$$X_i(0) = Lb + r \times (Ub - Lb) i = 1, 2, \ldots, n \tag{1}$$

where, r denotes a random integer range within [0, 1], n defines the individual count, $X(0)$ shows the initial location of the i^{th} individuals and Ub and Lb represent the upper and lower bounds of the searching range correspondingly. Then, the new generation can be measured by assessing objective value which is used to define the food availability for an individual.

Next, the process of establishing territory can be stimulated. The population is territorial so keystones with female bugs are placed in the territory. The objective value of individuals is alienated and stored in territories to offer n territories with n WSs, where the individuals are gathered with selected WSs from each group and their orders.

Then, the mating begins. According to this concept, a considerable number of keystones are involved following the search for females during mating. Two decisions were recognized: when a female can be attracted by the signals, then can react by conveying a signal, and then mating is started. Otherwise, mating is negated although keystones attempt to take forced mating; it cannot go that occurred because of the stronger shield on their body. The mathematical formula of this process can be given as follows:

$$\begin{cases} X_i(t+1) = X_i(t) + R \times r, & \textit{if mating happens} \\ X_i(t+1) = X_i(t) + R \times (1+r), & \textit{Otherwise} \end{cases} \tag{2}$$

In Eq. (2), $X_i(t)$ indicates the i^{th} WS position, and R shows the distance between the female territory ($X_F(t)$) and keystone position ($X_i(t)$):

$$R = X_F(t) - X_i(t) \tag{3}$$

Then, the foraging stage begins. They need to be reenergized for recovery dependent upon various efforts of the

WSs to be laid and breeding. This can be performed by finding a place with sufficient energy. Now, the main role define the existing location. When the objective values for the individual are higher than the prior location, then the novel food location could not be the best, otherwise, it passes over the optimal territory that involves the high fitness ($X_{BL}(t)$). The mathematical expression can be given as follows:

$$X_i^{t+1} = X_i(t) + 2 \times r(md \times (X_{BL}(t) - X_i(t)) \quad (4)$$

Eventually, in the end, phase (called succession and death), to maintain the performance in the finding boundaries, when there is an outlandish WS from the novel territory, the keystone gives a powerful performance to the newest member to bring him out or kill him. Some murdering (individuals eliminating) has happened due to the harsh behaviors. In this phase, compared to the new individual, if the previous location has a worse value, then the new individual was replaced and the WS was eliminated. Otherwise, the previous keystones have been kept, the newest one has been removed, and it could be specified as follows mathematically:

$$X_i^{t+1} = Lb_j(t) + r \times \left(Ub_j(t) - Lb_j(t)\right) \quad (5)$$

In Eq. (5), $Ub(t)$ and $Lb(t)$ refers the maximum and the minimum value of the position of the WS location during the *jth* territory.

Lastly, the process ends when the ending condition is attained.

In IWSA, the opposition-based learning method is integrated into the WSA, which is a popular technique for enhancing the efficacy of metaheuristics. The algorithm begins with a random population. Thus, an accurate solution will be achieved if the random primary population take the outcome nearer to the finest solution. Optimization starts with an arbitrary value far away from the better performance, or probably from the opposite place of the outcome that raises the time for the optimizer. The OBL technique offers an opposite place for the outcome from the primary population:

$$X_i^{OBL}(0) = X_i(0)^{max} + X_i(0)^{min} - X(0) \quad (6)$$

In Eq. (6), X_i^{0BL} defines the opposite position of X_i, and $X_i(0)$ max and $X_i(0)^{min}$ show the maximum and minimum boundaries of the difficult variable, correspondingly.

The newest place offers valuable opportunities with high probabilities for accomplishing better results. $X_i^{OBL}(0)$ is measured by the cost function and thus, if $X_i^{OBL}(0)$ is in the optimum place then $X_i(0)$, will be a sub-state.

The IWSA model generates a fitness function (FF) to achieve an increased classifier solution. This gives details of a positive integer for representing the better result of candidate performances. The decrease of classifier errors can be measured as FF.

$$fitness(x_i) = ClassifierErrorRate(x_i) = \frac{No.\ of\ misclassified\ instances}{Total\ no.\ of\ instances} * 100 \quad (7)$$

D. DETECTION USING CAE MODEL

At the final stage, the CAE approach can be employed for the classification of LCC. The most AE difference is the CAE, where an FC layer has been exchanged by the convolution layer [26]. CAEs have the benefits of either convolution layers or the unsupervised pre-trained ability of AE. Compared to the typical AE network, the CAE comprises convolution layers in the encoded and deconvolution layers rather than the FC layer from the decoded. The presented CAE comprises pooling, convolutional, and deconvolution layers. The encoded contains one convolutional and pooling layer. The decoded comprises of deconvolution layer. Encoded the performance of convolutional function with max-pooling layer allows higher level-layer representations which can be invariant to smaller input transmission as well as decrease the computational rate of the presented system. Fig. 2 demonstrates the framework of CAE. The convolution-deconvolution layers are subsequently an activation function that is defined as:

$$h^k = \sigma\left(\sum_{l \in L} x^l \otimes w^k + b^k\right) \quad (8)$$

whereas

h^k = *the* hidden representation of the k^{th} mapping feature of the present layer

x^l = *the* l^{th} mapping feature of the group of mapping features L acquired in the preceding layer

$\otimes$ = *a* 2*D* convolutional function

σ = *the* activation function

w^k = the weights of *the* k^{th} mapping feature of the present layer

b^k = the bias of k^{th} mapping features of the present layer "Valid convolutional" has been carried out via the convolutional layer, and "full convolutional" has been executed by the deconvolution layer. Additionally, once the dimension of mapping feature x^l is $p \times p$ and the filter dimension is $q \times q$, and then executing the valid convolutional, the dimension develops $(p - q+1) \times (p - q+1)$, and after executing the full convolutional, the dimension develops $(p + q - 1) \times (p + q - 1)$.

By exploiting the maximal activity in the input mapping features, a max-pooling layer pools features, and based on the dimension of the pooling kernel, this creates the decreased size of resultant mapping features.

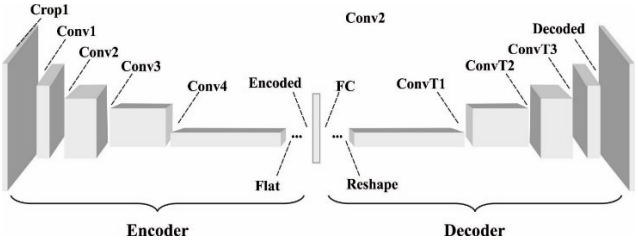

FIGURE 2. CAE structure.

IV. RESULTS AND DISCUSSION

The proposed model is simulated using Python 3.8.5 tool. The proposed model is experimented on PC i5-8600k, GeForce 1050Ti 4GB, 16GB RAM, 250GB SSD, and 1TB HDD. The performance analysis of the IWSACAE-LCCD system can

be performed with the LC25000 database [27], comprising 25000 data instances with 5 classes as described in Table 1. Sample images under every class are shown in Fig. 3.

TABLE 1. Description of database.

Classes	Description	No. of instances
Con-Adc	Colon Adenocarcinoma	5000
Con-BeT	Colon Benign Tissue	5000
Lug-Adc	Lung Adenocarcinoma	5000
Lug-BeT	Lung Benign Tissue	5000
Lug-Scc	Lung Squamous Cell Carcinoma	5000
Total No. of Instances		25,000

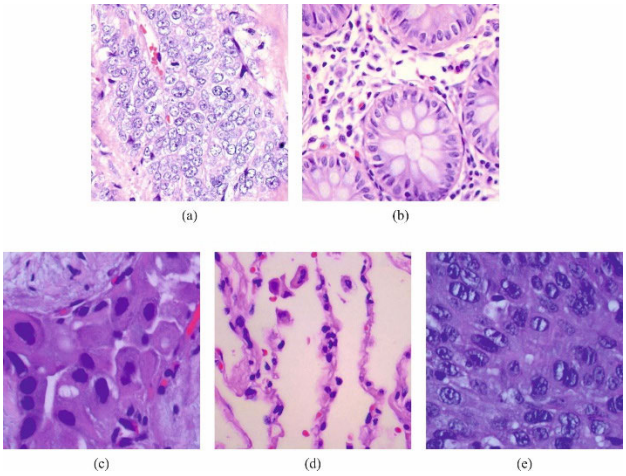

FIGURE 3. Sample images (a) Con-Adc, (b) Con-BeT, (c) Lug-Adc, (d) Lug-BeT, and (e) Lug-Scc.

A set of measures employed for examining the classification outcomes are accuracy ($accu_y$), precision ($prec_n$), recall ($reca_l$), and F-score (F_{score}).

$Prec_n$ evaluates the proportion of appropriately determined positive instances out of every instance that was represented as positive.

$$Prec_n = \frac{\text{TP}}{\text{TP} + \text{FP}} \tag{9}$$

where TP signifies true positive, FP refers false positive, TN refers true negative, and FN indicates false negative.

$Reca_l$ estimates the proportion of positive instances appropriately classified.

$$Reca_l = \frac{\text{TP}}{\text{TP} + \text{FN}} \tag{10}$$

$Accu_y$ computes the proportion of properly categorized instances (positives and negatives) against the total samples (No. of samples to be classified).

$$Accu_y = \frac{\text{TP} + \text{TN}}{\text{TP} + \text{TN} + \text{FP} + \text{FN}} \tag{11}$$

F_{score} determines integrating the harmonic mean of recall and precision.

$$F_{score} = \frac{2\text{TP}}{2\text{TP} + \text{FP} + \text{FN}} \tag{12}$$

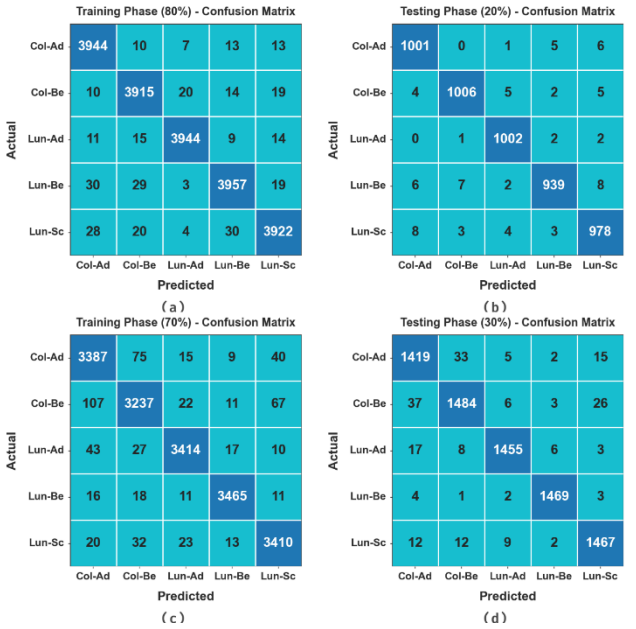

FIGURE 4. (a-b) Confusion matrices of IWSACAE-LCCD method 80:20 of TRS/TSS and (c-d) 70:30 of TRS/TSS.

Fig. 4 signifies the confusion matrices presented by the IWSACAE-LCCD algorithm with various datasets. The attained outcome defined by the IWSACAE-LCCD methodology can be precisely recognized and categorized into five classes.

In Table 2 and Fig. 5, the classification result of the IWSACAE-LCCD system with 80:20 of training set/testing set (TRS/TSS) can be represented in terms of diverse measures such as accuracy ($accu_y$), precision ($prec_n$), recall ($reca_l$), F-score (F_{score}), and AUC score (AUC_{score}). The achieved outcome demonstrated that the IWSACAE-LCCD method gains effectual recognition outcomes. According to 80% of TRS, the IWSACAE-LCCD algorithm provides an average $accu_y$ of 99.36%, $prec_n$ of 98.41%, $reca_l$ of 98.41%, F_{score} of 98.41%, and AUC_{score} of 99.01%. Also, on 20% of TSS, the IWSACAE-LCCD system achieves an average $accu_y$ of 99.41%, $prec_n$ of 98.52%, $reca_l$ of 98.51%, F_{score} of 98.51%, and AUC_{score} of 99.07%.

In Table 3 and Fig. 6, the classifier analysis of the IWSACAE-LCCD model in 70:30 of TRS/TSS can be depicted. These obtained outcomes implied that the IWSACAE-LCCD methodology achieves effectual recognition outcomes. On 70% of TRS, the IWSACAE-LCCD methodology gains an average $accu_y$ of 98.66%, $prec_n$ of 96.65%, $reca_l$ of 96.64%, F_{score} of 96.64%, and AUC_{score} of 97.90%. Similarly, with 30% of the TSS, the IWSACAE-LCCD model obtains an average $accu_y$ of 98.90%, $prec_n$ of 97.26%, $reca_l$ of 97.27%, and aF_{score} of 97.27%, and AUC_{score} of 98.29%.

TABLE 2. Classifier analysis of IWSACAE-LCCD model at 80:20 of TRS/TSS.

Class	$Accu_y$	$Prec_n$	$Reca_l$	F_{Score}	AUC_{Score}
TRS (80%)					
Con-Adc	99.39	98.04	98.92	98.48	99.21
Con-BeT	99.31	98.14	98.42	98.28	98.98
Lug-Adc	99.59	99.15	98.77	98.96	99.28
Lug-BeT	99.27	98.36	97.99	98.18	98.79
Lug-Scc	99.27	98.37	97.95	98.16	98.77
Average	99.36	98.41	98.41	98.41	99.01
TSS (20%)					
Con-Adc	99.40	98.23	98.82	98.52	99.18
Con-BeT	99.46	98.92	98.43	98.68	99.08
Lug-Adc	99.66	98.82	99.50	99.16	99.60
Lug-BeT	99.30	98.74	97.61	98.17	98.66
Lug-Scc	99.22	97.90	98.19	98.05	98.83
Average	99.41	98.52	98.51	98.51	99.07

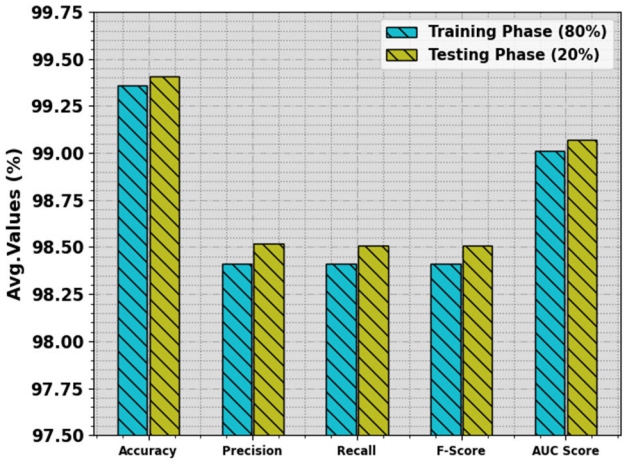

FIGURE 5. Average of IWSACAE-LCCD approach at 80:20 of TRS/TSS.

TABLE 3. Classifier outcome of IWSACAE-LCCD model at 70:30 of TRS/TSS.

Class	$Accu_y$	$Prec_n$	$Reca_l$	F_{Score}	AUC_{Score}
TRSs (70%)					
Con-Adc	98.14	94.79	96.06	95.42	97.36
Con-BeT	97.95	95.51	93.99	94.75	96.45
Lug-Adc	99.04	97.96	97.24	97.60	98.36
Lug-BeT	99.39	98.58	98.41	98.49	99.03
Lug-Scc	98.77	96.38	97.48	96.93	98.29
Average	98.66	96.65	96.64	96.64	97.90
TSS (30%)					
Con-Adc	98.33	95.30	96.27	95.78	97.55
Con-BeT	98.32	96.49	95.37	95.93	97.23
Lug-Adc	99.25	98.51	97.72	98.11	98.68
Lug-BeT	99.69	99.12	99.32	99.22	99.55
Lug-Scc	98.91	96.90	97.67	97.28	98.44
Average	98.90	97.26	97.27	97.27	98.29

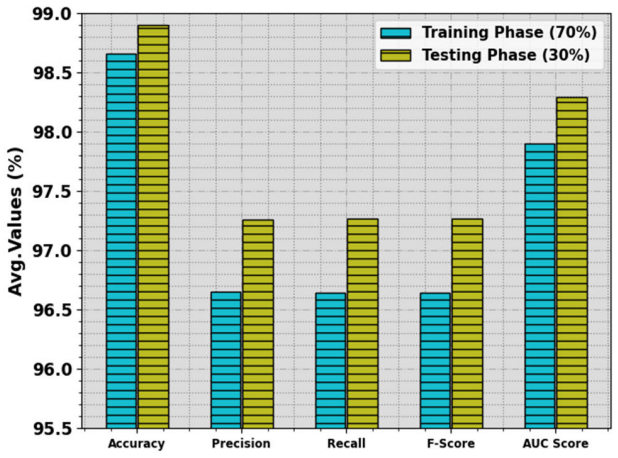

FIGURE 6. Average of IWSACAE-LCCD method at 70:30 of TRS/TSS.

Fig. 7 illustrates the training $accu_yTR\_accu_y$ and VL_accu_y of the IWSACAE-LCCD algorithm with 80:20 of the TRS/TSS. The TL_accu_y could be determined by the evaluation of the IWSACAE-LCCD approach at the TR database but the VL_accu_y can be evaluated the effectiveness under a distinct database of TS. The attained outcome displayed that TR_accu_y and VL_accu_y upsurge with epochs improvement. Therefore, the performance of the IWSACAE-LCCD model has improved with databases of TS and TR.

In Fig. 8, the *TR_loss* and *VR_loss* results of the IWSACAE-LCCD approach at 80:20 of the TRS/TSS are exhibited. The *TR_loss* defines the error among the original values and predictive solution under the data of TR. The *VR_loss* signify the evaluation of the IWSACAE-LCCD algorithm on specific validation data. The acquired outcome shows that the *TR_loss* and *VR_loss* get minimized with rising epochs. It gives the enriched effectiveness of the IWSACAE-LCCD system as well as its proficiencies for accurately making the classification. The minimal value

FIGURE 7. $Accu_y$ curve of IWSACAE-LCCD approach at 80:20 of TRS/TSS.

of *TR_loss* and *VR_loss* displays the excellent outcome of the IWSACAE-LCCD methodology under correlations and capturing patterns.

FIGURE 8. Loss curve of IWSACAE-LCCD system at 80:20 of TRS/TSS.

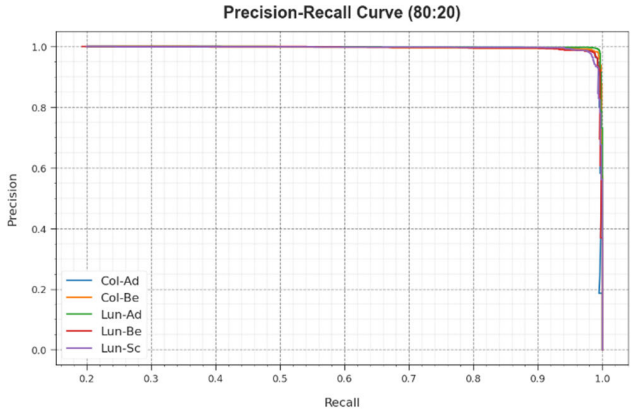

FIGURE 9. PR curve of IWSACAE-LCCD system at 80:20 of TRS/TSS.

In Fig. 9, a wide-ranging precision-recall (PR) analysis of the IWSACAE-LCCD technique can be under 80:20 of TRS/TSS. The accomplished findings display the IWSACAE-LCCD algorithm outcomes in higher PR outcomes. Then, it can be evident that the IWSACAE-LCCD methodology achieves greater effectiveness of PR with 5 classes.

In Fig. 10, a receiver operating characteristic curve (ROC) analysis of the IWSACAE-LCCD methodology can be displayed at 80:20 of the TRS/TSS. The attained outcome values of the IWSACAE-LCCD algorithm provide a greater value of ROC. Next, this can be noticeable that the IWSACAE-LCCD algorithm gets better performances of ROC on 5 classes.

A wide-ranging analysis of the IWSACAE-LCCD technique with other approaches can be ensured using a comparative result, as given in Table 4 [28]. The attained outcome values notified that the mSRC and ResNet50 models accomplished poor performance. Next to that, the MPADL-LC3, Faster R-CNN, and DAELGNN algorithms obtained moderately nearer results. Moreover, the BERTL-HIALCC technique reaches considerable performance with $anaccu_y$ of 99.10%, $prec_n$ of 97.96%, $reca_l$ of 97.94%, and F_{score} of 97.93%. However, the IWSACAE-LCCD technique resulted in maximum performance with $accu_y$ of 99.41%, $prec_n$ of 98.52%, $reca_l$ of 98.51%, and F_{score} of 98.51%.

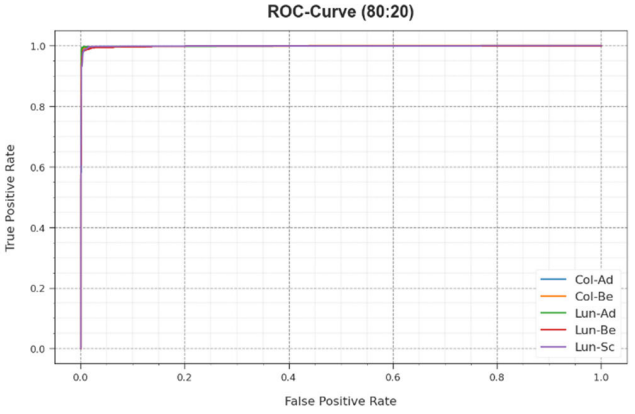

FIGURE 10. ROC analysis of IWSACAE-LCCD methodology at 80:20 of TRS/TSS.

TABLE 4. Comparison analysis of the IWSACAE-LCCD algorithm with other methodologies [28].

Methods	$Accu_y$	$Prec_n$	$Reca_l$	F_{Score}
IWSACAE-LCCD	99.41	98.52	98.51	98.51
BERTL-HIALCC	99.10	97.96	97.94	97.93
MPADL-LC3 Algorithm	98.96	97.89	97.09	96.96
mSRC	88.09	85.09	91.66	86.66
Faster R-CNN	98.66	96.42	97.51	97.20
DAELGNN	98.61	97.83	96.27	96.68
RESNET50	93.53	96.01	97.37	96.83

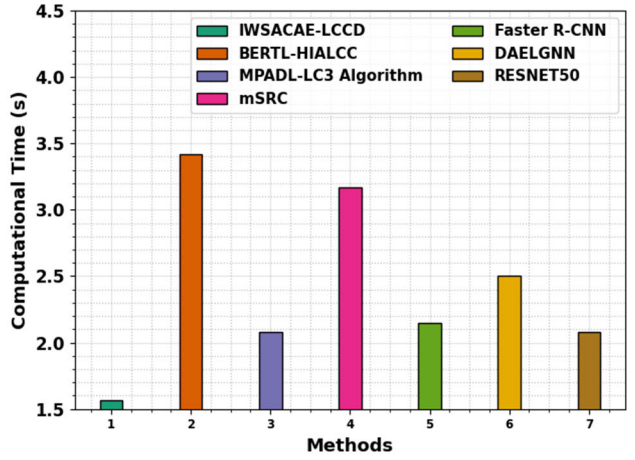

FIGURE 11. CT outcome of IWSACAE-LCCD system with other approaches.

Fig. 11 demonstrates the comparative computational time (CT) analysis of the IWSACAE-LCCD technique with other existing methods. The simulation value stated that the IWSACAE-LCCD technique obtains the least CT value of 1.57s. On the other hand, the BERTL-HIALCC, MPADL-LC3, mSRC, Faster R-CNN, DAELGNN, and RESNET50 techniques accomplished higher CT values of 3.42s, 2.08s, 3.17s, 2.15s, 2.50s, and 2.08s respectively.

Thus, the IWSACAE-LCCD algorithm can be employed for automated LCC detection.

V. CONCLUSION

In this manuscript, we considered the development of the IWSACAE-LCCD algorithm for the detection and classi-

fication of LCC on HIs. This proposed IWSACAE-LCCD method proposes to recognize and classify lung as well as colon cancers. In the presented IWSACAE-LCCD technique, MF-based preprocessing, MobileNetv2 feature extractor, IWSA-based hyperparameter tuning, and CAE-based cancer detection. The application of the IWSA model helps in the optimum selection of the hyperparameters related to the CAE algorithm that can be used which identifies the occurrence of lung as well as colon cancer. To enhance the detection results of the IWSACAE-LCCD technique, a series of simulations were performed. The achieved values emphasized that the IWSACAE-LCCD system gains superior outcomes over other systems. Future work can focus on accessing an enormous and diverse dataset of higher-quality HIs which can be important for training and validating DL models. Obtaining annotated data for cancer and non-cancer cases can be challenging, and data imbalance can affect model performance. In addition, the DL models need high computation resources for handling high-resolution HIs. Besides, deploying AI models in a clinical environment may require specialized hardware, such as GPUs or TPUs, which might not be readily available or compatible with existing systems.

ACKNOWLEDGMENT

The authors extend their appreciation to the Deanship of Scientific Research at King Khalid University for funding this work through large group Research Project under grant number (RGP2/248/44). Princess Nourah bint Abdulrahman University Researchers Supporting Project number (PNURSP2023R161), Princess Nourah bint Abdulrahman University, Riyadh, Saudi Arabia. Research Supporting Project number (RSPD2024R838), King Saud University, Riyadh, Saudi Arabia. This study is partially funded by the Future University in Egypt (FUE).

REFERENCES

[1] S. Tummala, S. Kadry, A. Nadeem, H. T. Rauf, and N. Gul, "An explainable classification method based on complex scaling in histopathology images for lung and colon cancer," *Diagnostics*, vol. 13, no. 9, p. 1594, Apr. 2023.

[2] G. Yu, K. Sun, C. Xu, X.-H. Shi, C. Wu, T. Xie, R.-Q. Meng, X.-H. Meng, K.-S. Wang, H.-M. Xiao, and H.-W. Deng, "Accurate recognition of colorectal cancer with semi-supervised deep learning on pathological images," *Nature Commun.*, vol. 12, no. 1, p. 6311, Nov. 2021.

[3] S. Mangal, A. Chaurasia, and A. Khajanchi, "Convolution neural networks for diagnosing colon and lung cancer histopathological images," 2020, *arXiv:2009.03878*.

[4] O. Stephen and M. Sain, "Using deep learning with Bayesian–Gaussian inspired convolutional neural architectural search for cancer recognition and classification from histopathological image frames," *J. Healthcare Eng.*, vol. 2023, pp. 1–9, Feb. 2023.

[5] A. B. Hamida, M. Devanne, J. Weber, C. Truntzer, V. Derangère, F. Ghiringhelli, G. Forestier, and C. Wemmert, "Deep learning for colon cancer histopathological images analysis," *Comput. Biol. Med.*, vol. 136, Sep. 2021, Art. no. 104730.

[6] Y. Tang, S. Liu, Y. Deng, Y. Zhang, L. Yin, and W. Zheng, "An improved method for soft tissue modelling," *Biomed. Signal Process. Control*, vol. 65, Mar. 2021, Art. no. 102367.

[7] S. Lu, B. Yang, Y. Xiao, S. Liu, M. Liu, L. Yin, and W. Zheng, "Iterative reconstruction of low-dose CT based on differential sparse," *Biomed. Signal Process. Control*, vol. 79, Jan. 2023, Art. no. 104204.

[8] S. Lu, S. Liu, P. Hou, B. Yang, M. Liu, L. Yin, and W. Zheng, "Soft tissue feature tracking based on deep matching network," *Comput. Model. Eng. Sci.*, vol. 136, no. 1, pp. 363–379, 2023.

[9] Y. Zhuang, S. Chen, N. Jiang, and H. Hu, "An effective WSSENet-based similarity retrieval method of large lung CT image databases," *KSII Trans. Internet Inf. Syst.*, vol. 16, no. 7, 2022.

[10] L. Sun, M. Zhang, B. Wang, and P. Tiwari, "Few-shot class-incremental learning for medical time series classification," *IEEE J. Biomed. Health Informat.*, pp. 1–11, 2023.

[11] B. K. Hatuwal and H. C. Thapa, "Lung cancer detection using convolutional neural network on histopathological images," *Int. J. Comput. Trends Technol.*, vol. 68, no. 10, pp. 21–24, Oct. 2020.

[12] G. Srivastava, A. Chauhan, and N. Pradhan, "CJT-DEO: Condorcet's jury theorem and differential evolution optimization based ensemble of deep neural networks for pulmonary and colorectal cancer classification," *Appl. Soft Comput.*, vol. 132, Jan. 2023, Art. no. 109872.

[13] R. D. Mohalder, J. P. Sarkar, K. A. Hossain, L. Paul, and M. Raihan, "A deep learning based approach to predict lung cancer from histopathological images," in *Proc. Int. Conf. Electron., Commun. Inf. Technol. (ICECIT)*, Sep. 2021, pp. 1–4.

[14] X. Xiao, Z. Wang, Y. Kong, and H. Lu, "Deep learning-based morphological feature analysis and the prognostic association study in colon adenocarcinoma histopathological images," *Frontiers Oncol.*, vol. 13, Feb. 2023, Art. no. 1081529.

[15] Y. Yang, J. Yang, Y. Liang, B. Liao, W. Zhu, X. Mo, and K. Huang, "Identification and validation of efficacy of immunological therapy for lung cancer from histopathological images based on deep learning," *Frontiers Genet.*, vol. 12, Feb. 2021, Art. no. 642981.

[16] R. R. Wahid, C. Nisa, R. P. Amaliyah, and E. Y. Puspaningrum, "Lung and colon cancer detection with convolutional neural networks on histopathological images," *Proc. AIP Conf. Proc.*, vol. 2654, no. 1, Feb. 2023.

[17] D. Z. Karim and T. A. Bushra, "Detecting lung cancer from histopathological images using convolution neural network," in *Proc. IEEE Region Conf. (TENCON)*, Dec. 2021, pp. 626–631.

[18] A. Saif, Y. R. H. Qasim, H. A. M. H. Al-Sameai, O. A. Farhan Ali, and A. A. M. Hassan, "Multi paths technique on convolutional neural network for lung cancer detection based on histopathological images," *Int. J. Adv. Netw. Appl.*, vol. 12, no. 2, pp. 4549–4554, 2020.

[19] H. A. Mengash, M. Alamgeer, M. Maashi, M. Othman, M. A. Hamza, S. S. Ibrahim, A. S. Zamani, and I. Yaseen, "Leveraging marine predators algorithm with deep learning for lung and colon cancer diagnosis," *Cancers*, vol. 15, no. 5, p. 1591, Mar. 2023.

[20] M. Chen, S. Huang, Z. Huang, and Z. Zhang, "Detection of lung cancer from pathological images using CNN model," in *Proc. IEEE Int. Conf. Comput. Sci., Electron. Inf. Eng. Intell. Control Technol. (CEI)*, Sep. 2021, pp. 352–358.

[21] S. Hadiyoso, S. Aulia, and I. D. Irawati, "Diagnosis of lung and colon cancer based on clinical pathology images using convolutional neural network and CLAHE framework," *Int. J. Appl. Sci. Eng.*, vol. 20, no. 1, pp. 1–7, 2023.

[22] Y. Qasim, H. Al-Sameai, O. Ali, and A. Hassan, "Convolutional neural networks for automatic detection of colon adenocarcinoma based on histopathological images," in *Proc. Int. Conf. Reliable Inf. Commun. Technol.* Cham, Switzerland: Springer, Dec. 2020, pp. 19–28.

[23] N. Kapoor, A. Gupta, and K. Meenakshi, "EfCNN-Net: Smart detection of colon and lung cancer using histopathological images," in *Proc. 3rd Int. Conf. Intell. Technol. (CONIT)*, Jun. 2023, pp. 1–6.

[24] Z. Xiaolong, J. Tian, and D. Hao, "A lightweight network model for human activity classifiction based on pre-trained MobileNetV2," Tech. Rep., 2021.

[25] L. Hu, Y. Zhang, and N. Yousefi, "Nonlinear modeling of the polymer membrane fuel cells using deep belief networks and modified water strider algorithm," *Energy Rep.*, vol. 7, pp. 2460–2469, Nov. 2021.

[26] D. Thakur, S. Biswas, E. S. L. Ho, and S. Chattopadhyay, "ConvAE-LSTM: Convolutional autoencoder long short-term memory network for smartphone-based human activity recognition," *IEEE Access*, vol. 10, pp. 4137–4156, 2022.

[27] A. A. Borkowski, M. M. Bui, L. B. Thomas, C. P. Wilson, L. A. DeLand, and S. M. Mastorides. *Lung and Colon Cancer Histopathological Image Dataset (LC25000)*. Accessed: Jul. 14, 2023. [Online]. Available: https://www.kaggle.com/datasets/andrewmvd/lung-and-colon-cancerhistopathological-images

[28] R. AlGhamdi, T. O. Asar, F. Y. Assiri, R. A. Mansouri, and M. Ragab, "Al-biruni earth radius optimization with transfer learning based histopathological image analysis for lung and colon cancer detection," *Cancers*, vol. 15, no. 13, p. 3300, Jun. 2023.